ADVANCED QUANTUM TECHNOLOGIES
www.advquantumtech.com

Optical Characterization of InGaN Quantum Structures at the Nanoscale

*Wai Yuen Fu and Hoi Wai Choi**

This review paper presents an overview of the optical characterization techniques for Indium Gallium Nitride (InGaN) quantum well (QW) structures at a nanoscale. The two major techniques are reviewed—Electron Microscopy-Cathodoluminescence (EM-CL) and Scanning Near-field Optical Microscopy (SNOM). It elucidates the critical role these methodologies play in revealing the complex properties of InGaN QWs, including their structural characteristics, optical properties, carrier dynamics, and the effects of defects and doping. The review highlights key findings from a variety of studies, demonstrating how EM-CL and SNOM have contributed to the understanding of these micro-/nano- structures and their potential applications in high-efficiency optoelectronic devices.

1. Introduction

III-Nitride-based devices, including light-emitting diodes (LEDs), laser diodes (LDs), and high-electron-mobility transistors (HEMTs), have permeated our daily lives, largely owing to the pioneering work of Nobel laureates S. Nakamura,[1,2] I. Akasaki[3,4] and H. Amano.[5,6] Their seminal contributions have led to the creation of high-quality InGaN heterostructures and have facilitated the effective incorporation and activation of p-dopants. The remarkable optical and electronic properties of III-Nitrides devices have spurred their wide adoption across various technologies, including light sources, displays, and chargers, with the global market anticipated to reach USD 28.3 billion by 2028.[7]

Emission characterization from III-Nitride materials and devices primarily hinges upon a diverse range of optical characterization techniques, which have formed the bedrock of research and development over numerous decades. Conventional microscopy techniques such as optical microscopy or atomic force microscopy are typically utilized to characterize sample geometry or morphology. While the understanding of geometry or morphology is paramount, the characterization of InGaN-based optoelectronic devices focuses predominantly on the emission from active regions, typically quantum wells or quantum dots, which are generally in the nanoscale. This necessitates the use of optical characterization techniques capable of exciting and/or extracting nanoscale light emissions from the active region.

These emissions can be catergorized into photoluminescence (PL), electroluminescence (EL), and cathodoluminescence (CL), corresponding to excitation by optical pumping, current injection, and electron beam, respectively. To facilitate nano-scale characterization, either the excitation or the collection technique must offer nanometer resolution, leading to the advent of various characterization techniques. Confocal microscopy/spectroscopy, though readily applicable for EL and PL much like conventional microscopy, remains limited by the diffraction limit (λ/2NA) of the received emission, despite the implementation of a confocal pinhole. Given that the emission from InGaN quantum structures typically spans the visible spectrum, the usual resolution limit is generally above 200 nm for a Numerical Aperture (NA) of 1, thereby not truly qualifying as nanoscale.

In a bid to circumvent the diffraction limit, the scanning near-field microscopy/spectroscopy technique was introduced. This technique, grounded in scanning probe microscopy, employs a tip that is either an aluminum (Al)-coated single-mode fiber or a subsequently apertured SiO_2 pyramid for light coupling in the near-field, thus allowing for a resolution beyond the diffraction limit, typically around 100 nm. For excitation with an electron beam, this is typically conducted within a scanning electron microscope or a transmission electron microscope. The mapping resolution relies solely on the interaction volume of the electron beam with the sample, as the collection of emitted light is performed in the far field. Nonetheless, electron microscopes, particularly tranmission electron microscope (TEM), typically achieve sub-10 nm resolution without the limitation of the optical source diffraction limit, rendering the achievable resolution generally higher.

In this review, we provide an overview of these two primary optical characterization techniques, Scanning Near-Field Optical Microscopy (SNOM) and electron microscope-CL, that have significantly contributed to the research and development of InGaN quantum structures. These techniques are not only useful for characterizing nanostructures, but they can also reveal nanoscale

W. Y. Fu, H. W. Choi
Department of Electrical and Electronic Engineering
the University of Hong Kong
Pokfulam Road, Hong Kong 999077, Hong Kong
E-mail: hwchoi@hku.hk

The ORCID identification number(s) for the author(s) of this article can be found under https://doi.org/10.1002/qute.202300335

DOI: 10.1002/qute.202300335

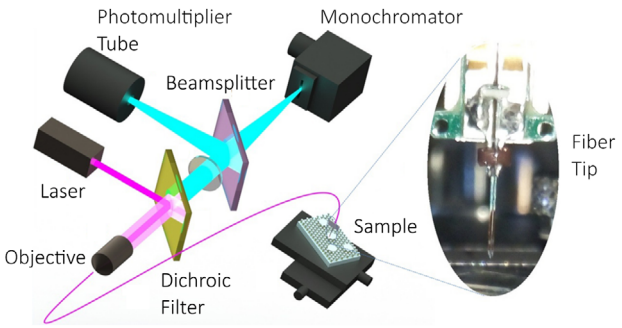

Figure 1. Schematic diagram of a SNOM/SNOS setup. Reproduced with permission.[16] Copyright 2016, American Chemical Society.

fluctuations from the emission of a micron-scale device, which could provide insights into the performance or mechanisms of the device.

2. SNOM

SNOM constitutes a powerful technique for nanoscale optical characterization, facilitating the exploration of light emission at scales far surpassing traditional diffraction limits. Initially proposed by E. H. Synge in 1928,[8] the fundamental concept of SNOM was first demonstrated by E. A. Ash and G. Nicholls in 1972,[9] albeit not at the nanoscale. The contemporary version of this technique, which has significantly influenced the field, was developed by D. W. Pohl in 1982.[10–12]

The essence of the SNOM technique lies in the utilization of a probe possessing an aperture of diameter smaller than its wavelength. This configuration allows for efficient coupling and focusing of light between the probe and the specimen. The aperture of the SNOM probe tip is typically coated with a metal such as Al, confining the light within the sub-wavelength domain of the tip aperture. In order to enhance the coupling efficiency and suppress radiation mode loss, a single-mode fiber is commonly employed.[13]

As the sample is scanned at a minimal distance beneath the aperture, the optical resolution of the transmitted or reflected light becomes limited by the diameter of the aperture, thus facilitating sub-wavelength resolution. This is achieved by harnessing the evanescent field, or near-field light, a non-propagating field that exists only within distances less than a single wavelength of light from the specimen surface and exponentially decays beyond that. By capturing this near-field light before diffraction takes place, SNOM can be used for spectroscopic analysis at nanoscopic optical spatial resolutions, constrained only by the size of the SNOM probe aperture. This spectroscopic technique is sometimes called scanning near-field optical spectroscopy (SNOS).[14] In practice, while a lateral resolution of 6 nm has been demonstrated,[15] the resolution of commercial SNOM is generally limited to about 100 nm. A schematic diagram of a typical SNOM/SNOS setup is demonstrated in **Figure 1**.

Depending on the experimental setup, there are four typical modes of SNOM operation: illumination (I) mode, collection (C) mode, illumination-collection (I-C) mode, and multi-probe (M) mode. In the illumination mode, a laser serves as the excitation source which is coupled, typically through a fiber, and focused through an aperture smaller than its own wavelength to excite the sample with high resolution. The excited photoluminescence (PL) signal is then collected from the far-field. The collection mode involves exciting a PL signal from the far-field, either from the side or the back of the specimen. This mode also allows direct current injection into the quantum structure for near-field EL signal collection by the SNOM probe. The illumination-collection mode, offering the highest spatial resolution, utilizes the same fiber probe for both the excitation and collection of the PL signal. However, as the excitation and collection positions are identical in this mode, a fourth multi-probe mode is introduced, typically used for studying carrier diffusion or photon propagation, particularly in the case of nitride optoelectronic devices. In this mode, a fixed aperture probe is positioned at a predetermined excitation location in the near-field, while the SNOM probe scans and collects the PL signal. With the evolution of SNOM technology, aperture less SNOM variants have emerged, leveraging tip or plasmon enhancement to further improve system resolution or throughput. Nevertheless, this paper will concentrate on aperture SNOM, given its widespread application in the study of InGaN quantum structures over the past decades.

2.1. Quantum Wells

To unravel the intricate nanoscale properties of InGaN QWs, SNOM has emerged as a frequently employed technique. SNOM offers unique insights into defects, inhomogeneities, and complex carrier interactions that govern emission and efficiency by facilitating optical characterization at a spatial resolution below the diffraction limit.

SNOM's primary use in the III-Nitride field is to illuminate the impacts of defects on efficiency and emission properties. Thanks to its capacity to extend optical characterization into the nanoscale resolution realm, there have been numerous reports of spatial inhomogeneity in emission.[17–21] These irregularities are typically attributed to dislocations and fluctuations in Indium composition. As for the former, early work by A. Vertikov et al.[22] suggested that strong carrier localisation in InGaN alloys might mitigate the adverse effects of dislocation on PL efficiency. G. Marutsuki et al.[23] conducted a SNOM-EL mapping with a configuration illustrated in **Figure 2** and found a correlation between regions of longer peak wavelength and stronger intensities, implying that injected carriers redistribute towards local potential minima. P.A. Crowell et al.[24] also found no correlation between dislocation-associated v-pits and PL fluctuations, albeit found no evidence for the recombination of strongly localized carriers. A. Kaneta et al. demonstrated that dislocations do not necessarily serve as major non-radiative recombination centers across samples with varying Indium compositions, as shown in UV-emitting[25] and blue-emitting[26] samples. K. Okamoto et al. also demonstrated identification radiation and non-radiation centers on an LED sample using SNOM-PL and SNOM-TRPL.[27]

Furthermore, H. Jeong et al. also highlighted differences in the distribution of luminescent centers on InGaN multiple quantum well (MQW) samples grown on sapphire and Gallium Nitride (GaN) substrates with respective dislocation densities.[30] Given subsequent reports of limited internal quantum efficiency (IQE)

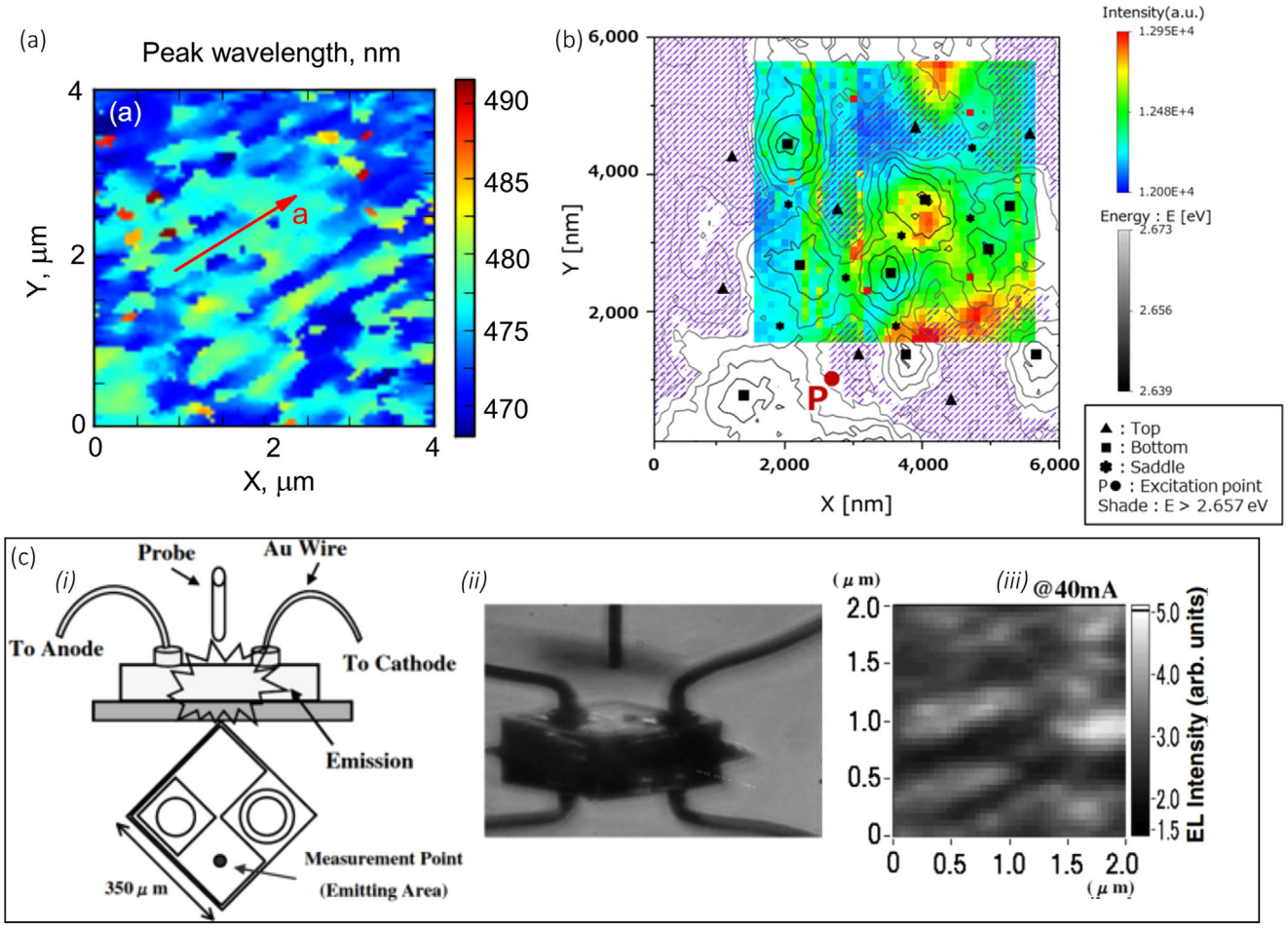

Figure 2. a) Near-field PL map showing emission features from semipolar QW aligning along the *a*-direction. Reproduced with permission.[28] Copyright 2013, AIP Publishing. b) Overlap from a near-field PL map of an InGaN/GaN MQWs under collection mode (contour) and multi-probe mode (colored). Reproduced under the terms of the CC BY license.[29] Copyright 2022, Nature Publishing Group. c, i) Schematics and ii) photos of SNOM-EL experiment, with iii) the SNOM-EL map on the right. Reproduced with permission.[23] Copyright 2002, John Wiley & Sons.

improvement upon further dislocation density reduction,[31] R. Yapparov et al. undertook a comprehensive analysis of polar InGaN/GaN films using multi-mode SNOM. They examined PL intensity, peak wavelength, and decay lifetime, and cross-referenced their findings with results from High-angle annular dark-field imaging (HAADF)–scanning TEM (STEM). Their research revealed that dislocation densities play a minimal role in InGaN sample IQEs, as only the immediate vicinity of v-pits, which account for a small percentage of the total QW area, is affected.[32]

SNOM's capability to conduct spectroscopic analyses at nanoscale spatial resolution has enabled researchers to uncover spatial inhomogeneities in InGaN QW emission. These irregularities primarily originate from inherent Indium composition fluctuations. An early study by A. Vertikov et al. associated PL fluctuations with Indium composition variations, particularly in relation to the size distribution of Indium clusters.[33] Subsequent research by J. Kim[34] and B. Han et al.[18] supported this correlation, noting that spatial variation in PL emission wavelength increases with a higher Indium composition, likely due to an increase in Indium composition fluctuation. In addition to Indium composition fluctuations, growth morphology also contributes to inhomogeneity in semipolar/nonpolar InGaN QWs. V. Liuolia et al. identified that localisation areas on an InGaN QW grown on an *m*-plane GaN substrate align with the [0001] direction due to partial strain relaxation at monolayer steps.[35] A. Kaneta et al. observed a local distribution of spectral red-shift correlated to the surface morphology of a $20\bar{2}1$ SQW on an *m*-plane GaN substrate.[36] Furthermore, S. Marcinkevicius et al.,[28] during their examination of a semipolar $20\bar{2}\bar{1}$ InGaN/GaN QW sample, observed a similar trend with the sub-micron emission features aligning along the *a*-direction, as illustrated in Figure 2.

To further probe carrier dynamics within InGaN QWs, researchers have employed multi-probe SNOM. As demonstrated by A. Kaneta et al.,[37] a dual-probe mode facilitates near-field excitation at one spot while another probe collects light in the near-field to form a map. The signal received primarily originates from carrier diffusion and photon generation from the excited spot, contrasting with the I-C mode. A. Sakurai et al. used multi-probe SNOM to study an InGaN/GaN MQW sample,[29] as demonstrated in Figure 2. They discovered a discontinuous change in the maps, likely related to carrier dynamics within the

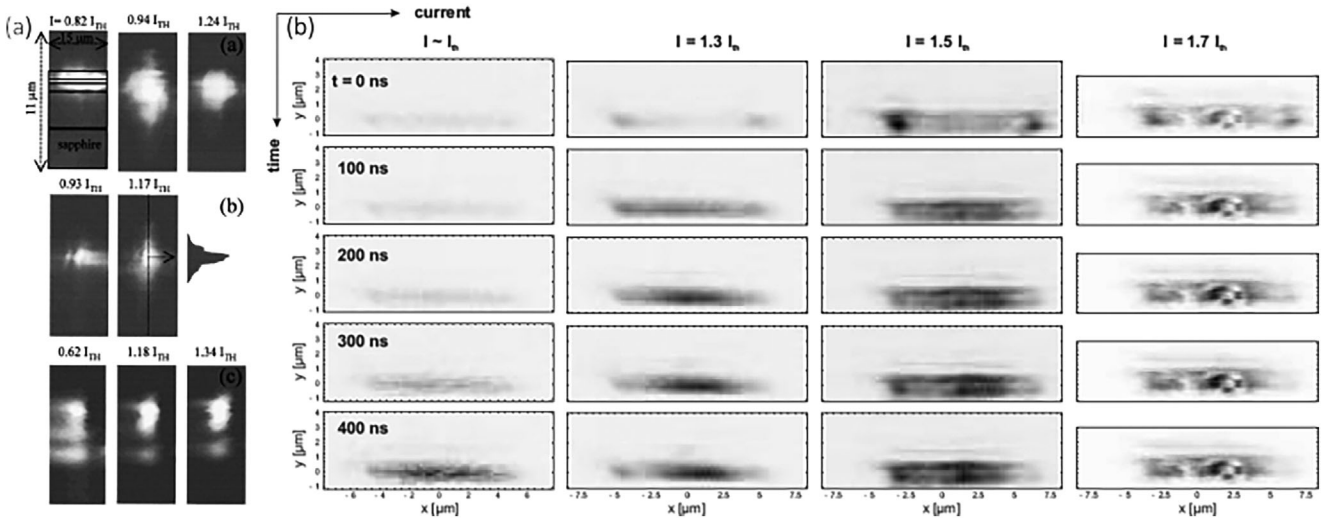

Figure 3. a) Near-field EL maps of an InGaN/GaN LD at different current density, normalized to the threshold current. Reproduced with permission.[38] Copyright 1999, AIP Publishing. b) Time-resolved near-field EL maps of an InGaN/GaN laser diode at different time. Reproducedwith permission.[40] Copyright 2006, SPIE.

sample, as discerned from the sliced intensity map of different emission energy ranges.

2.2. Lasers

Despite the technical challenges associated with experiments, the analysis of InGaN quantum well-based lasers through SNOM has been an area of sustained interest over several decades. In 1999, D. K. Young et al.[38] leveraged SNOM to investigate EL from both three and ten QW InGaN-based LDs. Their work offered a spatial resolution of less than 100 nm, enabling them to unveil phenomena such as absorption and re-emission of the lasing mode and correlations between modal emission, waveguide structure, and lateral device size. Notably, they observed that EL emission from the quantum well becomes confined to single-mode resonance as the current injection exceeds the lasing threshold, as shown in **Figure 3**. Similarly in 2016, S. Friede et al. analyzed the architectures of 420 nm emitting InGaN/GaN diode lasers by photoluminescence and photocurrent spectroscopy using a near-field scanning optical microscope.[39] They were able to individually inspect the components of the "optical active cavity", such as quantum wells, waveguides, and cladding layers. Their study revealed defect levels in the p-part of the waveguide and suggested that the homogeneity of the n-waveguide section directly affects the quantum wells grown on top of this layer.

J. C. Johnson et al.[40] reported an observation of ultraviolet-blue laser action in single monocrystalline GaN nanowires. They demonstrated that radiation patterns were correlated with axial Fabry–Perot modes, and a spectral red-shift was strongly dependent on pump power, supporting the hypothesis that the electron–hole plasma mechanism was principally responsible for the gain at room temperature. In 2005, U. T. Schwarz et al.[41] employed time-resolved SNOM to explore the evolution of the near-field and far-field of InGaN laser diode waveguide modes, offering insights into phenomena such as lateral mode competition, filamentation, and beam steering. A year later, they further extended their work to meticulously measure the mode dynamics of InGaN LDs emitting at 405 nm.[42] Their research contributed a wealth of observations, including mode competition, near-field phase dynamics, and substrate modes, significantly enriching the understanding of InGaN quantum well-based lasers.

2.3. Photonic Crystal

Despite a multitude of previous reports extolling the virtues of photonic crystals for enhancing LED light extraction, the consensus in the field now leans towards surface roughening as a more cost-effective solution with superior performance. Nevertheless, photonic crystal can still find use in the manipulation of optical modes and the formation of resonant cavities in the field of III-nitride.

J. Shakya et al.[43] used SNOM as part of their experimental setup to study III-nitride blue and ultraviolet (UV) photonic crystal LEDs. Their optical measurements led to observations of a 60° periodic variation with the angle between the propagation direction of emission light and the photonic crystal lattice. The study also highlighted a strong dependency of the optical enhancement factor on the photonic crystal lattice constant and hole size. Similarly, V. Liuolia et al.[44] employed both SNOM and time-resolved PL to investigate light extraction from InGaN photonic crystal LEDs. Their study reported complex near-field intensity patterns that did not correspond directly to the physical structure of the photonic crystal, suggesting that the photonic crystal not only improved the light extraction but also rendered the LED emission more homogeneous.

Z. Y. Fang et al.[45] fabricated two-dimensional micro-cylinder patterns of dodecagonal photonic quasi-crystal and tetragonal photonic crystal on the top surface of a GaN LED. SNOM was used to record and analyse the spatially resolved surface

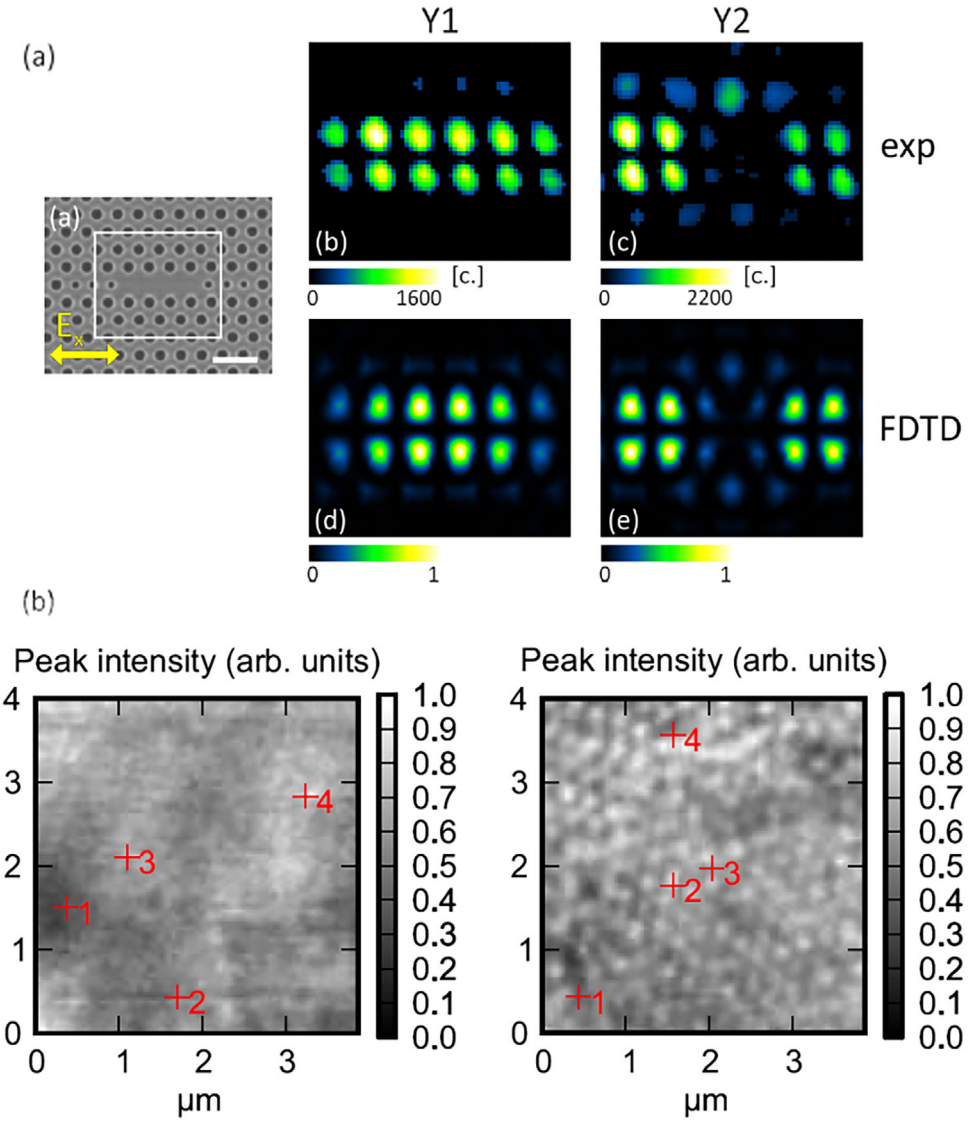

Figure 4. a) Near-field PL maps of a resonant mode inside a GaN-based photonic crystal cavity. Reproduced with permission.[46] 2015, AIP Publishing. b) Time-resolved near-field EL maps of an InGaN/GaN LD at different time. Reproduced with permission.[44] Copyright 2012, John Wiley & Sons.

emission. The study concluded that the light emission could be significantly enhanced due to surface plasmon resonance, with the enhancement factor for the dodecagonal photonic quasi-crystal being notably higher than that of the tetragonal photonic crystal and the non-patterned LED.

F. La China et al.[46] later used SNOM for deep sub-wavelength imaging of the vectorial components of the electric local density of states for the confined modes of a modified GaN L3 photonic crystal nanocavity. The mode mapping obtained with SNOM, as shown in **Figure 4** offered insights into the behaviors of photonic crystal nanocavities, with the experimental maps aligning well with numerical predictions.

Despite a multitude of previous reports extolling the virtues of photonic crystals for enhancing LED light extraction, the consensus in the field now leans towards surface roughening as a more cost-effective solution with superior performance. Nevertheless, photonic crystal can still find use in the manipulation of optical modes and the formation of resonant cavities in the field of III-nitride.

2.4. Microdisk

Characterization of InGaN quantum well-based microdisks using SNOM can be traced back to late 1990s, with the earliest research spearheaded by D. Lun et al.[47] This seminal work introduced $In_{0.22}Ga_{0.78}N$/ $In_{0.06}Ga_{0.94}N$ MQW microdisks, fabricated by photolithography and ion beam etching. SNOM was also employed in unveiling a pronounced emission preference along the radial direction of the microdisk, thereby indicating some evanescent emission being re-directed in the vertical direction by the micro-coupler.

In the same year, Y. Zhang et al.[48] reported on the fabrication of InGaN MQW microdisks with varying pivot diameters.

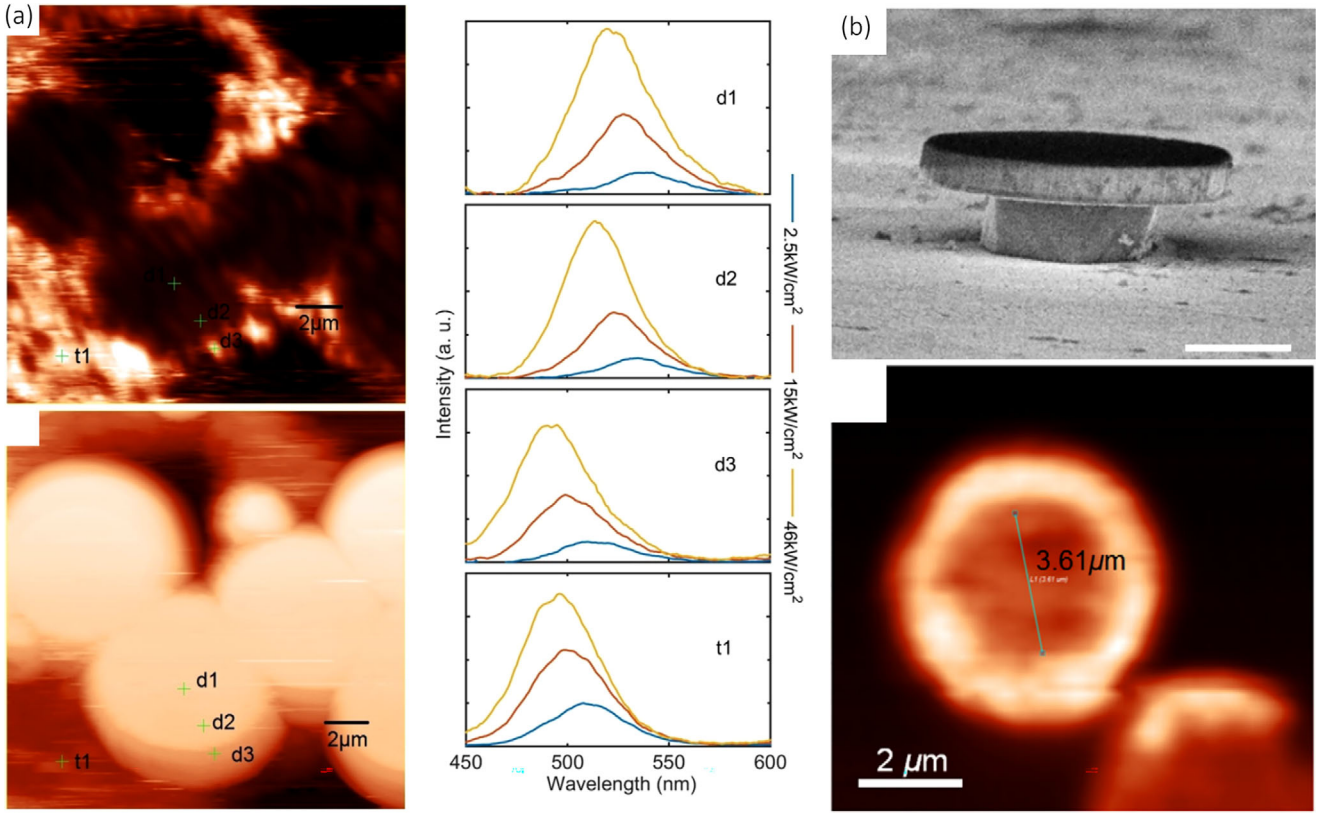

Figure 5. a) Near-field PL maps of microdisks with corresponding spectra taken from different positions. Reproduced with permission.[16] Copyright 2016, American Chemical Society. b) SEM image and corresponding near-field PL maps of a microdisk pivoted on Si substrate. Reproduced with permission.[48] Copyright 2016, IOP Publishing.

The authors noted significant differences in far-field and near-field fluorescence images. Particularly, the near-field mapping of the InGaN microdisks, as shown in **Figure 5**, exhibited a spectral blue-shift and an increase in emission near the microdisk's circumference. This was attributed to strain relaxation, resulting in a decrease in the quantum-confined Stark effect (QCSE).

C. Feng et al. in 2016[16] presented a monolithic phosphor-free broadband-emission light-emitting diode. This device combined high-density microstructured and nanostructured InGaN–GaN quantum wells, exploiting strain-relaxation induced by sizing in highly strained quantum wells. SNOM was employed to differentiate the PL spectra from individual nanotips and larger-dimensioned regions, as demonstrated in Figure 5. Similar blue-shift near the circumference of micropillar was observed. W. Y. Fu et al.[49] continued with a detailed study on the emission distribution on microdisk using SNOM and observed a noticeable red spectral shift at the edge of a low In-content microdisk. This shift was ascribed to a change in strain relaxation mechanism, as inferred from molecular dynamics simulations and TEM studies.

On the other hand, Y. Liu et al.[50] underlined the importance of understanding the measurement properties of the SNOM probe. This study highlighted the impact of probe tip diameter on the measurement of whispering gallery modes (WGMs), demonstrating that both nanometric and half-resonance-wavelength tips could yield high-contrast measurements, albeit with different interaction mechanisms

3. Electron Microscope - Cathodoluminescence (CL)

Cathodoluminescence (CL), a phenomenon often witnessed within the confines of a scanning electron microscope (SEM) or transmission electron microscope (TEM), encompasses the emission of light—spanning the visible to near-infrared spectrum—from a material exposed to high-energy electron bombardment.[51] This analytical technique, particularly efficacious in the characterisation and analysis of semiconductors, has firmly established itself as a formidable tool in the realm of material science.

The measurement process starts with the generation of primary electrons from the electron gun. They are subsequently accelerated towards the specimen and focused onto the sample surface through electromagnetic lenses. Following their excitation, the CL light emitted from the specimen is typically collected in the far-field, most commonly by a parabolic mirror. This light is then coupled to a spectrometer via an optical fiber for further analysis. A schematic diagram of the setup is shown in **Figure 6**.[52]

When a specimen is subjected to electron beam irradiation, the interaction of primary electrons with the specimen triggers inelastic scattering processes, which subsequently generate an excess of electrons and holes. These excess carriers then recombine, emitting photons in the process—a

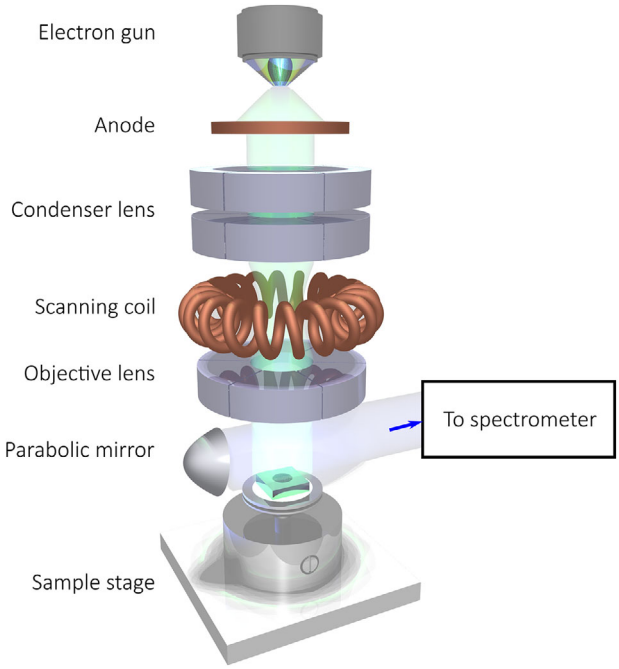

Figure 6. Schematic diagram of a conventional SEM-CL setup. The green and blue light denote the electron beam and CL light path, respectively.

spectacle duly captured for the purposes of imaging and spectroscopy.

Electron beams employed in an SEM or TEM can typically achieve a spot size less than 10 nm, unfettered by the diffraction limitations that constrain their optical beam counterparts. Nonetheless, it is important to note that the ultimate spatial resolution is not dictated by the beam size alone. Rather, it is determined by the interaction volume and the diffusion of excess charge carriers. The interaction volume can mainly be controlled by the acceleration voltage, while the diffusion of carriers can be influenced substantially by factors such as defect density, doping level, and charge carrier concentration.

3.1. Quantum Wells

The utilisation of cathodoluminescence (CL) within scanning electron microscope (SEM) and transmission electron microscopy (TEM) has significantly bolstered our understanding of InGaN quantum wells. SEM-CL and TEM-CL have progressively revealed the intricate dynamics of photons and charge carriers within these structures, which has proven beneficial for their optimisation in optoelectronic applications.

Understanding the impact of defects on the optical properties of InGaN quantum wells was a significant early focus of CL studies. T. Sugahara et al.[53] recognized the role of dislocations in luminescence in InGaN grown on sapphire substrates, leading to an understanding of their contribution as non-radiative recombination centers. The role of dislocations, both screw- and edge-type, were further investigated in the works of D. Cherns et al.[54] and S. J. Henley et al.,[55] highlighting the role of these defects in nonradiative recombination and quantum well emission degradation. Pozina et al.[56] later showcased how CL spatial mapping could elucidate the role of threading dislocations as nonradiative recombination centers at high injection conditions.

X. H. Wu et al.[57] also reported on the threading dislocation-related "V-defect", common to nearly all InGaN MQW heterostructures, finding its correlation with localised excitonic recombination centers. Thereafter, the study of defects and their impact on optical properties remained a critical area of inquiry. The work of D. I. Florescu et al.[58] on V-defects and inclusions in InGaN/GaN MQWs provided significant insights into the role of localised strain-energy variations in the occurrence of inclusions. Similarly, Y. E. Gmili et al.[59] conducted a comparative study of optical, morphological, microstructural, and microcompositional properties of typical InGaN samples, revealing the localized nature of luminescence peaks regarding V-defects. G. Kusch et al.[60] later extended the CL techniques to investigate the carrier dynamics at trench defects in InGaN quantum wells. T. Zhu et al.,[61] on the other hand, studied step bunch on *m*-plane InGaN/GaN MQW with SEM-CL, and found that the semi-polar QW at the step bunch exhibit a lower emission energy with longer decay time constant.

With advancing insights into the role of threading dislocations, it has been revealed that enhancements in IQE become limited as threading dislocation density diminishes.[31] This is due to the increasing impact of point defects acting as non-radiative recombination centers within the material.[62] Consequently, T.F.K. Weatherley et al.[63] employed the CL technique to image and characterise non-radiative point defects in QWs. The sample under study was grown on a *c*-plane free-standing GaN substrate, chosen to minimise interference from dislocations. By juxtaposing with secondary-electron (SE) imagery, dark spots in the CL images, which correspond to dislocations, have been accurately identified, thus isolating those corresponding to non-radiative point defects. This intriguing method for characterising point defects is particularly effective in samples with low threading dislocation density. However, it is important to note that a direct comparison with SE images alone may lead to an overestimation of point defect density, as edge-type dislocations might not be fully accounted for in this analysis.

The correlation between structural features and optical properties was also a recurring theme in this period. In the late 1990s, S. Chichibu et al.[64] identified strong exciton localisation in InGaN SQWs. Existence of quantum disk was observed in InN-rich area due to compositional undulation of InGaN/GaN SQW. X. Zhang et al.[65] revealed local band gap variations due to local In composition fluctuations and segregation during the growth process. Similarly, S. F. Chichibu et al.[66] and K. Uchida et al.[67] demonstrated how variations in well thickness, InN molar fraction, and doping could influence the emission mechanisms of strained InGaN quantum wells.

In more recent years, the field has seen further advancements in the use of CL to study InGaN quantum wells. P. R. Edwards et al.[68] introduced a novel approach combining wavelength-dispersive X-ray (WDX) microanalysis with CL spectral mapping, as shown in **Figure 7**. S. Sonderegger et al.[69] used atomic force microscopy (AFM) and picosecond time-resolved CL (TRCL) measurements to study InGaN/GaN quantum wells. They observed a contrast inversion between monochromatic CL maps corresponding to the high and low energy sides of the QW luminescence peak, suggesting that spectral diffusion from high

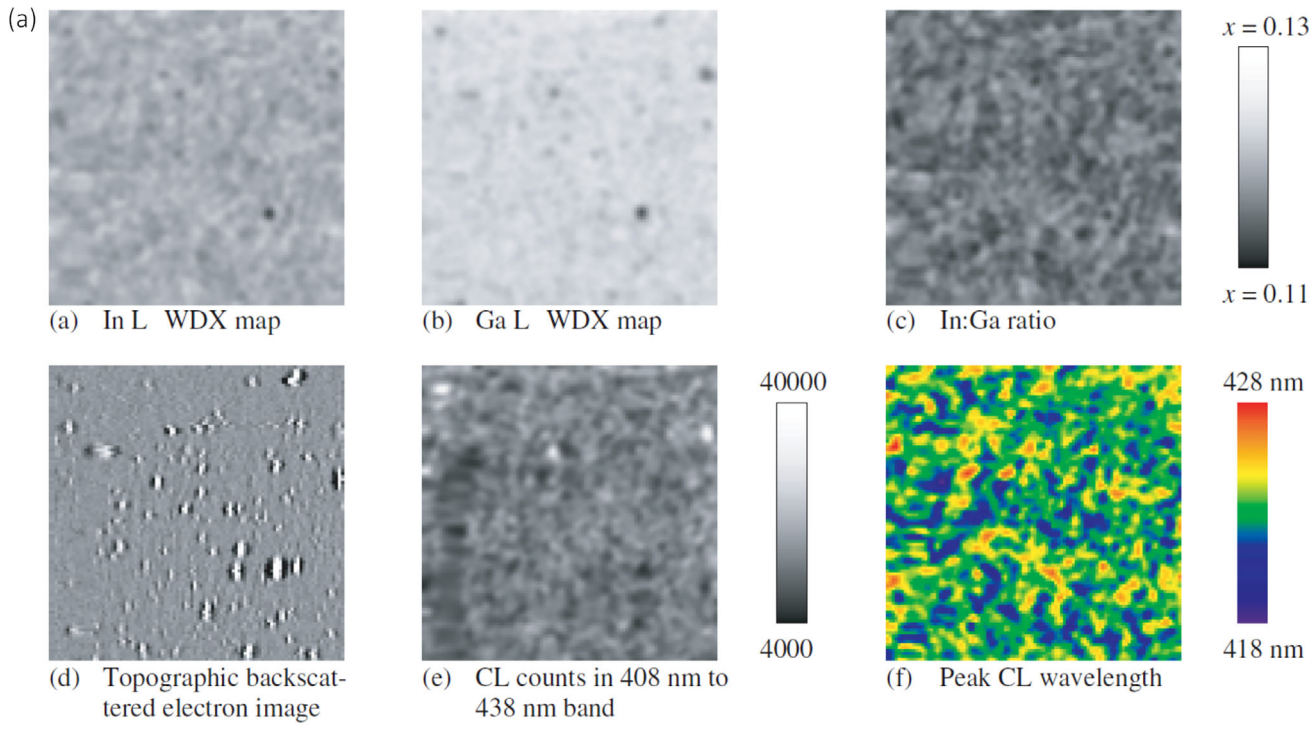

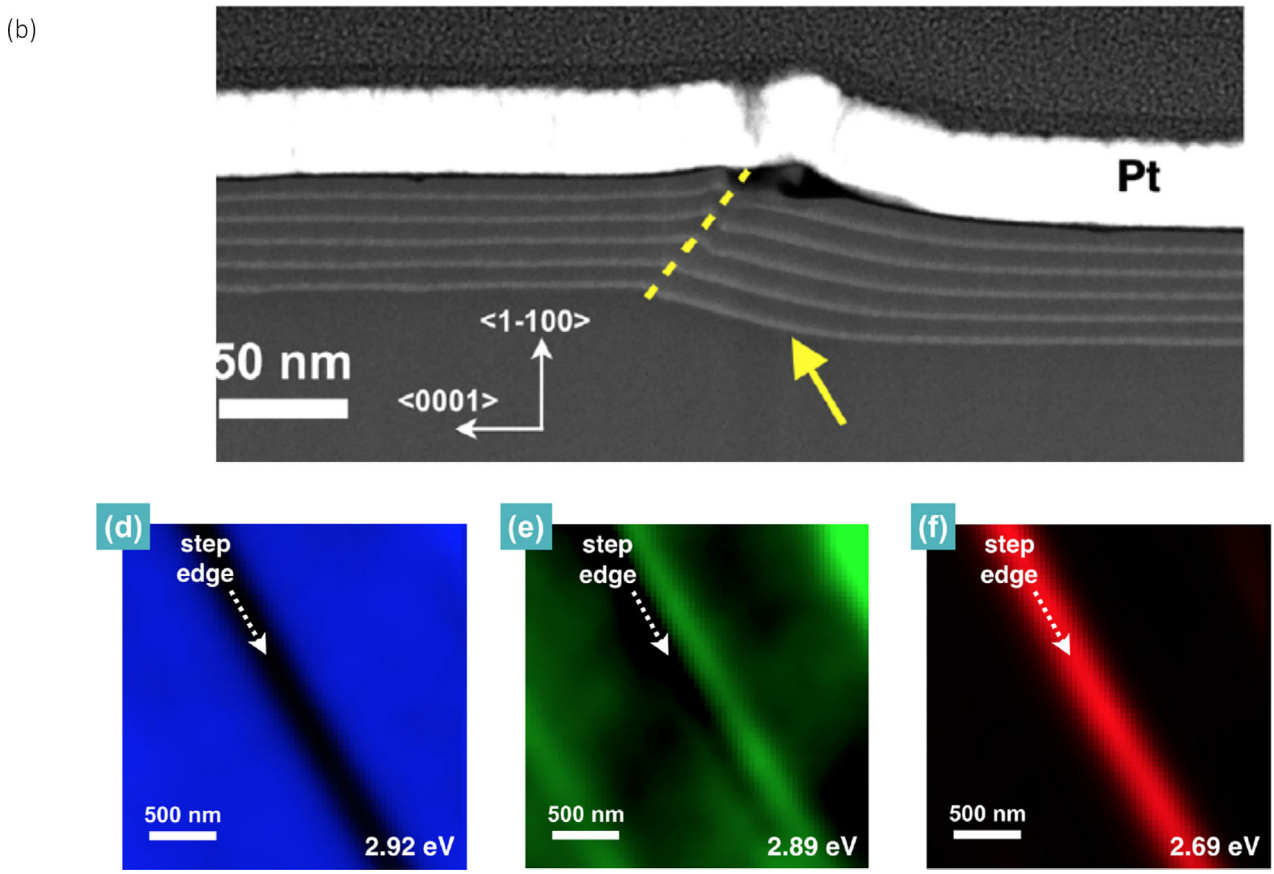

Figure 7. a) WDX and CL maps acquired simultaneously at the same position. Reproduced with permission.[68] Copyright 2003, John Wiley & Sons. b) CL maps of different emission energies collected at the same position near a step bunch on a *m*-plane MQW sample. Reproduced with permission.[61] Copyright 2016, AIP Publishing.

energy thinner regions to low energy thicker regions could potentially hinder nonradiative recombination at dislocations. J. Christen et al.[70] underscored the importance of a systematic nanoscale correlation of structural, chemical, electronic, and optical properties for a comprehensive understanding of semiconductor heterostructures. Using a newly developed SE-SEM-CL system, M. Yoshikawa et al.[71] provided further insights into the spectral properties of InGaN QWs and the CL spectral variations in the vicinity of the V-defects, respectively. More recent advancements in the field have been reported by S. F. Chichibu et al.,[72] who introduced the concept of spatio-time-resolved CL (STRCL), and S. Finot et al.,[73] who accessed the impact of nonradiative surface recombinations in micro-LEDs using photon-correlated CL.

The use of SEM-CL and TEM-CL in characterizing InGaN quantum wells has significantly advanced our understanding of these complex semiconductor systems. From the early discoveries of exciton localization and the role of defects, to the more recent advancements in simultaneous WDX with hyperspectral imaging and STRCL, these techniques have proven instrumental in unveiling the intricate behavior of photons and charge carriers within these structures. As our understanding of these systems continues to deepen, it is anticipated that further advancements in CL techniques will continue to drive discoveries in the field, particularly in light of the ongoing development and optimization of optoelectronic devices such as high-performance microdisplays based on III-nitride micro-LEDs.

3.2. Nanowires

Early research highlighted the importance of correlating structural characteristics with optical properties in InGaN nanowires. J. R. Riley et al.[74] in 2013 used atom probe tomography, cross-sectional STEM, and CL spectroscopy to analyze the InGaN/GaN MQWs in nanowire array LEDs. The team found that the position-dependent CL emission wavelength of the nonpolar side-facet QWs and semipolar top QWs correlated with the In composition. Similarly, M. Tchernycheva et al.[75] investigated a core-shell InGaN/GaN nanowire using SEM-CL, which reveals a decrease of CL intensity, attributing to the composition gradient in the InGaN QW, from bottom to top. W. Liu et al.[76] later utilized time-resolved CL to study the optical properties of InGaN/GaN core-shell microrods, and found that the non-radiative recombination lifetime decreased from the bottom to the top of the microrod due to an increased In-content in the upper part of the rod, leading to a higher density of point defects. Similarly, L. Yan et al.[77] examined the role of the microstructure and optical properties of InGaN/GaN nanowire LED structures on Si(111) with varying nanowire coverage. Their findings revealed that the bandgap emission coming from the GaN root was more pronounced, but attributing to higher numbers of stacking faults-related defected as less coalescence formation when the coverage of nanowires decreased.

Likewise, Y.-H. Ra et al.[78] in 2014 investigated the growth behavior of coaxial nonpolar (*m*-plane) and semipolar (*r*-plane) oriented MQWs on core n-GaN nanowires. Their power-dependent CL measurements revealed a defective interface between the *m*- and *r*-planes. The team then further explored the impact of crystal orientation on the performance of nanowire-based devices by comparing *m*-plane and *c*-plane oriented InGaN/GaN MQW nanowire LEDs[79] and found that the *m*-plane oriented MQW nanowire LEDs exhibited superior electrical properties due to the absence of piezoelectric polarization fields. This work underscored the importance of considering crystal orientation in the design of high-performance LEDs. Y.-H. Ra et al.[80] later reported on the fabrication of highly efficient p-type GaN nanocrystals using selective area epitaxial growth (SAG). The resulting p-contacted InGaN/GaN nanowire LEDs showed a low turn-on voltage, reduced resistance, and enhanced electroluminescence intensity, presenting a promising pathway towards high-efficiency InGaN LEDs.

More recently, G. Kusch et al.[81] used CL hyperspectral imaging to investigate spatial variations in the luminescence properties of InGaN/GaN core-shell microrods, as shown in **Figure 8**. They found that the luminescence properties could be modulated by cavity modes. On the other hand, A. Concordel et al.[82] estimated the defect concentration in nanowires through the statistical analysis of CL intensities across an ensemble of nanowires. By positing a Poisson distribution of non-radiative point defects, they have calculated the point defect density using the distribution of integrated CL intensities from individual nanowires. The study presupposes several conditions, including the random distribution of point defects adhering to Poisson statistics, uniformity in nanowire dimensions, indium incorporation, and quantum well width. Unfortunately, these assumptions do not invariably hold true. For instance, B. Ding et al.[83] have reported gross well width fluctuations[84] in QWs through combined SEM-CL and STEM investigations. While further empirical evidence might be required to substantiate the model's accuracy, the applicability of this methodology is primarily confined to smaller nanowires, as the distribution of point defects begins to deviate from Poisson's statistics in the presence of defect clustering.

These findings have laid the groundwork for the development of high-efficiency nanowire-based optoelectronic devices, such as LEDs, signalling a promising future for the field of InGaN nanowire research.

3.3. STEM-CL

One of the primary applications of STEM-CL in the study of InGaN nanowires is the direct correlation of structural and optical properties. This was demonstrated by S. K. Lim et al.,[85] who used STEM-CL to study the optical properties of single III-V nitride nanowire radial heterostructures. They observed enhanced carrier recombination in nanowire quantum wells and reduced light emission from regions containing structural defects, directly correlating these optical properties with structural characteristics.

In a study by G. Schmidt et al.[86] in 2014, STEM-CL was used to investigate the optical and structural properties of a 62 InGaN/GaN multiple quantum well embedded in an AlInN/GaN based microcavity. The researchers observed a spectral redshift between the individual quantum wells toward the surface of the nanowire, demonstrating the ability of STEM-CL to spatially resolve such shifts and link them to structural properties such as layer thickness.

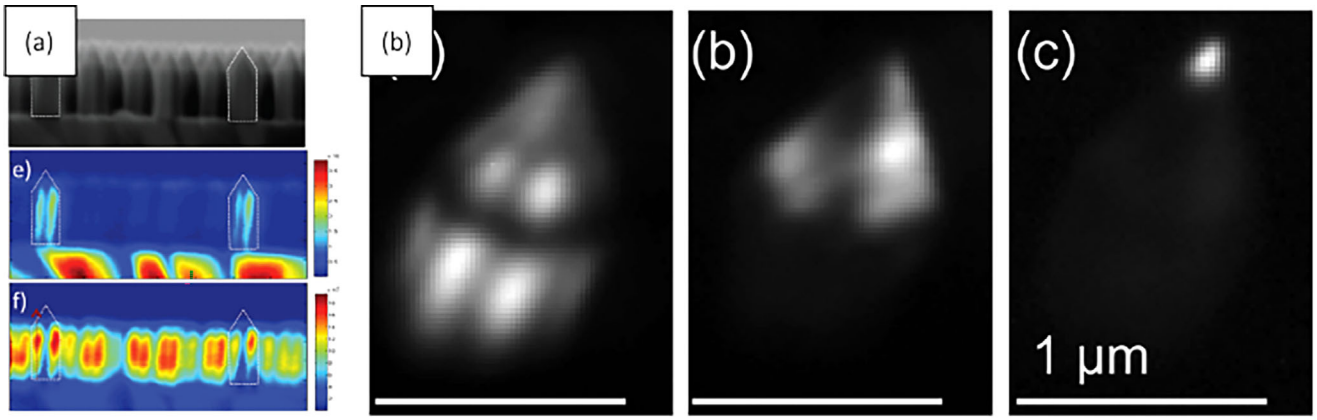

Figure 8. a) SEM image of nanowires and corresponding CL maps spectrally filtered at GaN band edge energies and QW emissions respectively. Reproduced under the terms of the CC BY license.[75] Copyright 2015, The Royal Society of Chemistry. b) CL maps of the apex of a InGaN/GaN nanorod, spectrally filtered at GaN near band edge emissions, semipolar QW emission and *c*-plane QW emission, respectively. Reproduced under the terms of the CC BY license.[81] Copyright 2018, Nature Publishing Group.

STEM-CL has also provided valuable insights into carrier recombination and trapping processes in InGaN nanowires. J. I. Deitz et al.[87] used STEM-CL to characterise two nanowire heterostructure types: a polarization-graded AlGaN nanowire light-emitting diode (LED) with a GaN quantum disk and a polarization-graded AlGaN nanowire with three different InGaN quantum disks. They found that the nanowires exhibited asymmetrical emission consistent with the polarization-induced electric fields in the barrier regions of the nano-LEDs. This work demonstrated the capability of STEM-CL to probe dynamic behaviours such as carrier recombination and trapping in these structures. Also importantly, J. T. Griffiths et al.[88] studied the spectral properties of individual quantum wells in an InGaN/GaN MQWs sample, and discovered a correlation of the emission wavelength with the Si doping concentration profile, as shown in **Figure 9**. The team[89] later investigated damage on InGaN QWs induced by electron beam using a similar technique, and found a decrease in CL intensity after exposure to e-beam above the damage threshold. The non-radiative region extends over the measured minority carrier diffusion length.

Similarly, W. Yi et al.[90] performed a systematic optical and structural characterization of quantum wells in core–shell GaN nanowires using CL and STEM. They found that the quantum wells grown on the *m*-facet showed varied optical behavior with respect to height position, with different regions exhibiting

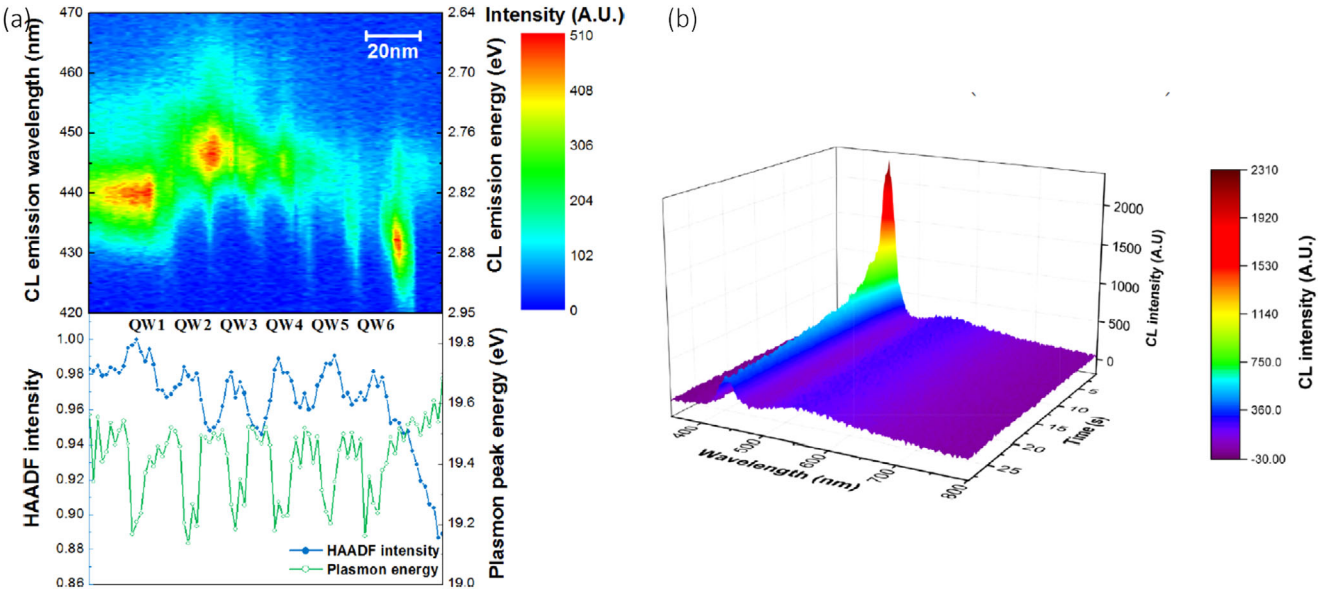

Figure 9. a) STEM-CL mapping of an InGaN/GaN MQW, showing each QW has a different emission spectrum that has a correlation with the Si doping profile. Reproduced under the terms of the CC BY license.[88] Copyright 2015, American Chemical Society. b) Decline in intensity of CL emission over time from InGaN MQWs exposed to an electron probe of 200 kV. Reproduced with permission.[89] Copyright 2016, AIP Publishing.

distinct luminescence behaviors. These variations were attributed to interface quality and In diffusion, demonstrating the utility of STEM-CL in linking optical behaviors to specific structural features.

4. Comparison of the SNOM and CL Techniques

The pursuit of advanced nanoscale characterization has spurred the evolution of sophisticated optical techniques, each transcending the constraints of traditional optics. This paper reviews two salient methodologies–SNOM and CL–which furnish unique capabilities and encounter particular challenges within this sphere. Here we meticulously assess the relative strengths and weaknesses of each technique, thereby illuminating their respective roles in the characterisation of cutting-edge materials.

In the realm of resolution, both SEM-CL and, to a greater extent, STEM-CL, command a significant advantage. This superiority stems from the electron beam's intrinsic high resolution, attributed to the narrow interaction volume with the sample. Notably, within the confines of quantum structures, the electrons are further constrained, enhancing the resolution in proximity to these formations. Consequently, CL emerges as a superior instrument for defect analysis, particularly in semiconductor materials where the presence and nature of defects are paramount in determining material performance.

Conversely, SNOM leverages near-field interactions to surpass the diffraction limit, with its resolving power being largely contingent upon the dimensions of the probe tip, which is generally larger than that of AFM due to the necessity of facilitating light transmission. In addition, the presence of quantum structures beneath the sample surface can further compromise SNOM's resolution, as signals emanating from greater depths may stray from the near-field domain.

The versatility of SNOM is exemplified by its ability to accommodate various excitation sources, such as lasers and electrical currents, enabling the collection of PL and EL signals, respectively. This adaptability renders SNOM particularly suited to examining the interplay between quantum structures and the entire device. Furthermore, the ability to have a fixed excitation source, combined with the collection of the excited near-field signal via the scanning probe tip, render SNOM a valuable instrument for observing resonant modes. Such modal analysis is challenging or even unattainable with SEM/STEM-CL, which necessitates scanning the sample with a nanoscale electron beam while collecting signals in the far-field.

To encapsulate, SNOM and CL each bear distinct advantages for optical characterisation at the nanoscale. The choice between these techniques should be predicated on the investigation's specific demands. Although CL generally prevails in terms of resolution, SNOM provides insights that more closely mirror operational conditions encountered in real-world applications. Typically, CL is the preferred method for analyzing epitaxial growth and microstructures that emerge during the growth process, while SNOM is frequently utilised to characterize optoelectronic device operations. Indeed, the synergistic application of SNOM and CL can potentially yield the most comprehensive insights, amalgamating their collective strengths to drive forward the understanding and advancement of InGaN quantum structures.

5. Conclusion

The application of EM-CL and SNOM in characterizing InGaN-based QW structures has significantly enriched the understanding of their micro-/nano- structures. These methodologies have been instrumental in shedding light on the intricate interplay between the structural characteristics, optical properties, and carrier dynamics within InGaN QWs and nanostructures. This review has highlighted key advancements and findings, including how these techniques have helped elucidate the influence of crystal orientation, the role of structural defects, and the impact of factors such as Indium composition and Si doping on the performance of InGaN QWs. Moreover, the evolution of techniques like SEM-CL and SNOM has enabled more detailed and nuanced investigations, paving the way for the potential use of InGaN QWs in high-efficiency nano-optoelectronic devices.

Acknowledgements

This work was jointly supported by a General Research Fund (Project 17206922) and the ANR/RGC Joint Research Scheme (Project A_HKU703/17) sponsored by the Research Grant Council of Hong Kong SAR.

Conflict of Interest

The authors declare no conflict of interest.

Keywords

CL, InGaN, SNOM, quantum well

Received: September 30, 2023
Revised: February 20, 2024
Published online:

[1] S. Nakamura, Y. Harada, M. Seno, *Appl. Phys. Lett.* **1991**, *58*, 2021.
[2] S. Nakamura, M. Senoh, T. Mukai, *Appl. Phys. Lett.* **1993**, *62*, 2390.
[3] I. Akasaki, H. Amano, K. Itoh, N. Koide, K. Manabe, *Inst. Phys. Conf. Ser.* **1992**, *129*, 851.
[4] I. Akasaki, H. Amano, M. Kito, K. Hiramatsu, *J. Lumin.* **1991**, *48*, 666.
[5] H. Amano, N. Sawaki, I. Akasaki, Y. Toyoda, *Appl. Phys. Lett.* **1986**, *48*, 353.
[6] H. Amano, M. Kito, K. Hiramatsu, I. Akasaki, *Jpn. J. Appl. Phys.* **1989**, *28*, L2112.
[7] ResearchAndMarkets.com, GaN semiconductor device market by type (opto-semiconductor, RF semiconductor, power semiconductor), device (discrete, integrated, hemt, mmic), application (lighting and lasers, power drives), voltage range, vertical and region - global forecast to 2028, https://www.researchandmarkets.com/report/gan-device. (accessed: March, 2024)
[8] E. H. Synge, *Lond., Edinburgh, Dublin Philos. Mag. J. Sci.* **1928**, *6*, 356.
[9] E. A. Ash, G. Nicholls, *Nature* **1972**, *237*, 510.
[10] D. W. Pohl, W. Denk, M. Lanz, *Appl. Phys. Lett.* **1984**, *44*, 651.
[11] U. Dürig, D. W. Pohl, F. Rohner, *J. Appl. Phys.* **1986**, *59*, 3318.
[12] D. W. Pohl, Optical near-field scanning microscope, **1982**.
[13] E. Betzig, *Principles and Applications of Near-Field Scanning Optical Microscopy (NSOM)*, Springer Netherlands, Dordrecht **1993**, pp. 7–15.

[14] V. F. Dryakhlushin, in *13th International Crimean Conference Microwave and Telecommunication Technology, 2003*. CriMiCo, Sevastopol, Ukraine 2003, **2003**, pp. 29–31.
[15] X. Ma, Q. Liu, N. Yu, D. Xu, S. Kim, Z. Liu, K. Jiang, B. M. Wong, R. Yan, M. Liu, *Nat. Commun.* **2021**, *12*, 6868.
[16] C. Feng, J.-A. Huang, H. W. Choi, *ACS Photonics* **2016**, *3*, 1294.
[17] S. Tripathy, S. J. Chua, In C. Gorecki, A. K. Asundi, editors, *Optical Micro- and Nanometrology in Manufacturing Technology*, International Society for Optics and Photonics, vol. *5458*, SPIE, Bellingham, WA **2004**, pp. 155–162.
[18] B. Han, B. W. Wessels, M. P. Ulmer, *J. Appl. Phys.* **2006**, *99*, 8.
[19] A. Kaneta, T. Izumi, K. Okamoto, Y. Kawakami, S. Fujita, Y. Narita, T. Inoue, T. Mukai, *Jpn. J. Appl. Phys.* **2001**, *40*, 110.
[20] A. Kaneta, G. Marutsuki, K. Okamoto, Y. Kawakami, Y. Nakagawa, G. Shinomiya, T. Mukai, S. Fujita, *Phys. Status Solidi B* **2001**, *228*, 153.
[21] K. Yoichi, O. Kunimichi, K. Akio, O. Koichi, N. Yukio, M. Takashi, F. Shigeo, *J. Phys.: Condens. Matter* **2001**, *13*, 6993.
[22] A. Vertikov, M. Kuball, A. V. Nurmikko, Y. Chen, S.-Y. Wang, *Appl. Phys. Lett.* **1998**, *72*, 2645.
[23] G. Marutsuki, Y. Narukawa, T. Mitani, T. Mukai, G. Shinomiya, A. Kaneta, Y. Kawakami, S. Fujita, *Phys. Status Solidi A* **2002**, *192*, 110.
[24] P. A. Crowell, D. K. Young, S. Keller, E. L. Hu, D. D. Awschalom, *Appl. Phys. Lett.* **1998**, *72*, 927.
[25] A. Kaneta, D. Yamada, G. Marutsuki, Y. Narukawa, T. Mukai, Y. Kawakami, *Phys. Status Solidi C* **2005**, *2*, 2728.
[26] A. Kaneta, M. Funato, Y. Kawakami, *Phys. Rev. B* **2008**, *78*, 125317.
[27] K. Okamoto, A. Scherer, Y. Kawakami, *Appl. Phys. Lett.* **2005**, *87*, 16.
[28] S. Marcinkevičius, Y. Zhao, K. M. Kelchner, S. Nakamura, S. P. DenBaars, J. S. Speck, *Appl. Phys. Lett.* **2013**, *103*, 13.
[29] A. Sakurai, K. Iwamoto, Y. Miwa, H. Hori, A. Ishikawa, K. Uchiyama, K. Kobayashi, K. Kishino, M. Sakai, *Sci. Rep.* **2022**, *12*, 10348.
[30] H. Jeong, H. J. Jeong, H. M. Oh, C.-H. Hong, E.-K. Suh, G. Lerondel, M. S. Jeong, *Sci. Rep.* **2015**, *5*, 9373.
[31] M. Shatalov, W. Sun, A. Lunev, X. Hu, A. Dobrinsky, Y. Bilenko, J. Yang, M. Shur, R. Gaska, C. Moe, G. Garrett, M. Wraback, *Appl. Phys. Express* **2012**, *5*, 082101.
[32] R. Yapparov, Y. C. Chow, C. Lynsky, F. Wu, S. Nakamura, J. S. Speck, S. Marcinkevičius, *J. Appl. Phys.* **2020**, *128*, 22.
[33] A. Vertikov, A. V. Nurmikko, K. Doverspike, G. Bulman, J. Edmond, *Appl. Phys. Lett.* **1998**, *73*, 493.
[34] J. Kim, K. Samiee, J. O. White, J.-M. Myoung, K. Kim, *Appl. Phys. Lett.* **2002**, *80*, 989.
[35] V. Liuolia, A. Pinos, S. Marcinkevičius, Y. D. Lin, H. Ohta, S. P. DenBaars, S. Nakamura, *Appl. Phys. Lett.* **2010**, *97*, 15.
[36] A. Kaneta, Y.-S. Kim, M. Funato, Y. Kawakami, Y. Enya, T. Kyono, M. Ueno, T. Nakamura, *Appl. Phys. Express* **2012**, *5*, 102104.
[37] A. Kaneta, T. Hashimoto, K. Nishimura, M. Funato, Y. Kawakami, *Appl. Phys. Express* **2010**, *3*, 102102.
[38] D. K. Young, M. P. Mack, A. C. Abare, M. Hansen, L. A. Coldren, S. P. Denbaars, E. L. Hu, D. D. Awschalom, *Appl. Phys. Lett.* **1999**, *74*, 2349.
[39] S. Friede, J. W. Tomm, S. Kühn, V. Hoffmann, H. Wenzel, M. Weyers, *Semicond. Sci. Technol.* **2016**, *31*, 115015.
[40] J. C. Johnson, H.-J. Choi, K. P. Knutsen, R. D. Schaller, P. Yang, R. J. Saykally, *Nat. Mater.* **2002**, *1*, 106.
[41] U. T. Schwarz, in *Frontiers in Optics*, OSA Technical Digest Series, Optica Publishing Group, Washington **2005**, p. FTuA2.
[42] U. Schwarz, C. Lauterbach, M. Schillgalies, C. Rumbolz, M. Furitsch, A. Lell, V. Härle, *Time-resolved scanning near-field microscopy of InGaN laser diode dynamics*, SPIE Photonics Europe, vol. 6184, SPIE, Bellingham, WA**2006**.
[43] J. Shakya, K. H. Kim, T. Oder, J. Y. Lin, H. X. Jiang, *III-nitride blue and UV photonic-crystal light-emitting diodes*, Optical Science and Technology, the SPIE 49th Annual Meeting, vol. *5530*, SPIE, Bellingham, WA **2004**.
[44] V. Liuolia, S. Marcinkevičius, Q. Wang, J. Andersson, S.-M. Kim, J. H. Baek, *Phys. Status solidi c* **2012**, *9*, 1664.
[45] Z. Fang, T. Dai, Q. Fu, B. Zhang, X. Zhu, *J. Microsc.* **2009**, *235*, 138.
[46] F. La China, F. Intonti, N. Caselli, F. Lotti, A. Vinattieri, N. Vico Triviño, J.-F. Carlin, R. Butté, N. Grandjean, M. Gurioli, *Appl. Phys. Lett.* **2015**, *107*, 10.
[47] D. Lun, B.-W. Zhang, Y. Zhang, R. P. Wang, X. Zhu, J. Lin, H. Jiang, *Optical Properties of InGaN Multiple Quantum Well Microdisks*, International Symposium on Photonics and Applications, vol. 3899, SPIE, Bellingham, WA**1999**.
[48] Y. Zhang, J.-A. Huang, K. H. Li, D. Bai, Y. Wang, T. Wang, H. W. Choi, *J. Phys. D: Appl. Phys.* **2016**, *49*, 375103.
[49] W. Y. Fu, H. W. Choi, *Optica* **2018**, *5*, 765.
[50] Y. Liu, S. Kadoya, M. Michihata, S. Takahashi, *Meas. Sci. Technol.* **2022**, *33*, 095501.
[51] B. G. Yacobi, D. B. Holt, *J. Appl. Phys.* **1986**, *59*, R1.
[52] K. Loeto, *Mater. Sci. Technol.* **2022**, *38*, 780.
[53] T. Sugahara, M. Hao, T. Wang, D. Nakagawa, Y. Naoi, K. Nishino, S. Sakai, *Jpn. J. Appl. Phys.* **1998**, *37*, L1195.
[54] D. Cherns, S. J. Henley, F. A. Ponce, *Appl. Phys. Lett.* **2001**, *78*, 2691.
[55] S. J. Henley, D. Cherns, *J. Appl. Phys.* **2003**, *93*, 3934.
[56] G. Pozina, R. Ciechonski, Z. Bi, L. Samuelson, B. Monemar, *Appl. Phys. Lett.* **2015**, *107*, 25.
[57] X. H. Wu, C. R. Elsass, A. Abare, M. Mack, S. Keller, P. M. Petroff, S. P. DenBaars, J. S. Speck, S. J. Rosner, *Appl. Phys. Lett.* **1998**, *72*, 692.
[58] D. I. Florescu, S. M. Ting, J. C. Ramer, D. S. Lee, V. N. Merai, A. Parkeh, D. Lu, E. A. Armour, L. Chernyak, *Appl. Phys. Lett.* **2003**, *83*, 33.
[59] Y. E. Gmili, G. Orsal, K. Pantzas, A. Ahaitouf, T. Moudakir, S. Gautier, G. Patriarche, D. Troadec, J. P. Salvestrini, A. Ougazzaden, *Opt. Mater. Express* **2013**, *3*, 1111.
[60] G. Kusch, E. J. Comish, K. Loeto, S. Hammersley, M. J. Kappers, P. Dawson, R. A. Oliver, F. C. P. Massabuau, *Nanoscale* **2022**, *14*, 402.
[61] T. Zhu, D. Gachet, F. Tang, W. Y. Fu, F. Oehler, M. J. Kappers, P. Dawson, C. J. Humphreys, R. A. Oliver, *Appl. Phys. Lett.* **2016**, *109*, 232103.
[62] M. Pristovsek, A. Bao, R. A. Oliver, T. Badcock, M. Ali, A. Shields, *Phys. Rev. Appl.* **2017**, *7*, 064007.
[63] T. F. K. Weatherley, W. Liu, V. Osokin, D. T. L. Alexander, R. A. Taylor, J.-F. Carlin, R. Butté, N. Grandjean, *Nano Lett.* **2021**, *21*, 5217.
[64] S. Chichibu, K. Wada, S. Nakamura, *Appl. Phys. Lett.* **1997**, *71*, 2346.
[65] X. Zhang, D. H. Rich, J. T. Kobayashi, N. P. Kobayashi, P. D. Dapkus, *Appl. Phys. Lett.* **1998**, *73*, 1430.
[66] S. F. Chichibu, A. C. Abare, M. P. Mack, M. S. Minsky, T. Deguchi, D. Cohen, P. Kozodoy, S. B. Fleischer, S. Keller, J. S. Speck, J. E. Bowers, E. Hu, U. K. Mishra, L. A. Coldren, S. P. DenBaars, K. Wada, T. Sota, S. Nakamura, *Mater. Sci. Eng., B* **1999**, *59*, 298.
[67] K. Uchida, T. Tang, S. Goto, T. Mishima, A. Niwa, J. Gotoh, *Appl. Phys. Lett.* **1999**, *74*, 1153.
[68] P. R. Edwards, R. W. Martin, K. P. O'Donnell, I. M. Watson, *Phys. Status Solidi C* **2003**, *n/a*, 2474.
[69] S. Sonderegger, E. Feltin, M. Merano, A. Crottini, J. F. Carlin, R. Sachot, B. Deveaud, N. Grandjean, J. D. Ganière, *Appl. Phys. Lett.* **2006**, *89*, 23.
[70] J. Christen, T. Riemann, F. Bertram, D. Rudloff, P. Fischer, A. Kaschner, U. Haboeck, A. Hoffmann, C. Thomsen, *Phys. Status Solidi C* **2003**, *n/a*, 1795.
[71] M. Yoshikawa, M. Murakami, H. Ishida, H. Harima, *Appl. Phys. Lett.* **2009**, *94*, 13.
[72] S. F. Chichibu, Y. Ishikawa, K. Hazu, K. Furusawa, *Jpn. J. Appl. Phys.* **2020**, *59*, 020501.
[73] S. Finot, C. Le Maoult, E. Gheeraert, D. Vaufrey, G. Jacopin, *ACS Photonics* **2022**, *9*, 173.

[74] J. R. Riley, S. Padalkar, Q. Li, P. Lu, D. D. Koleske, J. J. Wierer, G. T. Wang, L. J. Lauhon, *Nano Lett.* **2013**, *13*, 4317.
[75] M. Tchernycheva, V. Neplokh, H. Zhang, P. Lavenus, L. Rigutti, F. Bayle, F. H. Julien, A. Babichev, G. Jacopin, L. Largeau, R. Ciechonski, G. Vescovi, O. Kryliouk, *Nanoscale* **2015**, *7*, 11692.
[76] W. Liu, C. Mounir, G. Rossbach, T. Schimpke, A. Avramescu, H.-J. Lugauer, M. Strassburg, U. Schwarz, B. Deveaud, G. Jacopin, *Appl. Phys. Lett.* **2018**, *112*, 5.
[77] L. Yan, S. Jahangir, S. A. Wight, B. Nikoobakht, P. Bhattacharya, J. M. Millunchick, *Nano Lett.* **2015**, *15*, 1535.
[78] Y.-H. Ra, R. Navamathavan, S. Kang, C.-R. Lee, *J. Mater. Chem. C* **2014**, *2*, 2692.
[79] Y.-H. Ra, R. Navamathavan, H.-I. Yoo, C.-R. Lee, *Nano Lett.* **2014**, *14*, 1537.
[80] Y.-H. Ra, C.-R. Lee, *ACS Photonics* **2019**, *6*, 2397.
[81] G. Kusch, M. Conroy, H. Li, P. R. Edwards, C. Zhao, B. S. Ooi, J. Pugh, M. J. Cryan, P. J. Parbrook, R. W. Martin, *Sci. Rep.* **2018**, *8*, 1742.
[82] A. Concordel, N. Rochat, A. M. N. Quach, J.-L. Rouvière, G. Jacopin, J. Napierala, B. Daudin, *Nanotechnology* **2023**, *34*, 495702.
[83] B. Ding, J. Jarman, M. J. Kappers, R. A. Oliver, *J. Phys. D: Appl. Phys.* **2021**, *54*, 165107.
[84] R. A. Oliver, F. C.-P. Massabuau, M. J. Kappers, W. A. Phillips, E. J. Thrush, C. C. Tartan, W. E. Blenkhorn, T. J. Badcock, P. Dawson, M. A. Hopkins, D. W. E. Allsopp, C. J. Humphreys, *Appl. Phys. Lett.* **2013**, *103*, 14.
[85] S. K. Lim, M. Brewster, F. Qian, Y. Li, C. M. Lieber, S. Gradečak, *Nano Lett.* **2009**, *9*, 3940.
[86] G. Schmidt, M. Müller, P. Veit, F. Bertram, J. Christen, M. Glauser, J.-F. Carlin, G. Cosendey, R. Butté, N. Grandjean, *Appl. Phys. Lett.* **2014**, *105*, 3.
[87] J. I. Deitz, A. T. M. G. Sarwar, S. D. Carnevale, T. J. Grassman, R. C. Myers, D. W. McComb, *Microsc. Microanal.* **2018**, *24*, 93.
[88] J. T. Griffiths, S. Zhang, B. Rouet-Leduc, W. Y. Fu, A. Bao, D. Zhu, D. J. Wallis, A. Howkins, I. Boyd, D. Stowe, M. J. Kappers, C. J. Humphreys, R. A. Oliver, *Nano Lett.* **2015**, *15*, 7639.
[89] J. T. Griffiths, S. Zhang, J. Lhuillier, D. Zhu, W. Y. Fu, A. Howkins, I. Boyd, D. Stowe, D. J. Wallis, C. J. Humphreys, R. A. Oliver, *J. Appl. Phys.* **2016**, *120*, 165704.
[90] W. Yi, J. Uzuhashi, J. Chen, T. Kimura, S. Kamiyama, T. Takeuchi, T. Ohkubo, T. Sekiguchi, K. Hono, *Appl. Phys. Express* **2019**, *12*, 085003.

Wai Yuen Fu is a research assistant professor with the Department of Electrical and Electronic Engineering at The University of Hong Kong. He received his B.Eng. and M.Phil. degrees in electrical and electronic engineering from the University of Hong Kong and his Ph.D. degree in materials science from University of Cambridge (UK) under the supervision of Prof. Sir Colin Humphreys with a sponsorship of the Croucher scholarship. He then worked as a Postdoctoral Fellow in the University of Hong Kong supervised by Prof. HW Choi. His research focuses on modelling, characterization and fabrication of nano-optoelectronic devices based on III-V semiconductors.

Hoi Wai Choi is a professor with the Department of Electrical and Electronic Engineering at The University of Hong Kong. He received his Ph.D. from the National University of Singapore under the supervision of Professor Soo Jin Chua and completed his postdoctoral training in Professor Martin Dawson's team at the University of Strathclyde, Glasgow, where he contributed to pioneering development work on III-Nitride emissive micro-light-emitting diode arrays, demonstrating applications in the areas of micro-displays and high-efficiency light sources.